Geomagnetically Induced Current Calculation of High Voltage Power System with Long Transmission Lines using Kriging Method

# Geomagnetically Induced Current Calculation of High Voltage Power System with Long Transmission Lines using Kriging Method

Yu-hao Chen, Yan-zhao Xie, *Senior Member*, Min-zhou Liu, Zong-yang Wang, Qing Liu, Ai-ci Qiu

***Abstract*—Calculation of geomagnetically induced current (GIC) flowing through power system during the geomagnetic storm has attracted more attention recently. However, for high voltage power systems with transmission lines over hundreds or even thousands of kilometers, the earth model and geomagnetical field generally vary significantly. So, it is essential to take them into consideration using limited earth survey sites and geomagnetic observatories. To address this problem, a Kriging method is introduced in this paper to make earth model and geomagnetical field interpolations. It has the characteristic of spatial autocorrelation by considering not only the distances between predicted points and training points but also the distances between training points themselves. Finally, a case study of the Central China 1000 kV ultra-high voltage (UHV) grid is carried out to illustrate the applicability and effectiveness of the proposed method.**

***Index Terms*—Geomagnetically induced current, Kriging method, variation of earth model and geomagnetic field, 1000 kV UHV power grid.**

## I. Introduction

GEOMAGNETICALLY induced current (GIC) caused by geomagnetical disturbance (GMD) could be a potential threat to the power system. Once the transformer is led to half-cycle saturation by GIC, transformer overheating, misoperation of protective relays, voltage instability may happen subsequently. Even the power grid may collapse if several transformers or reactive power compensation devices are out of service in this circumstance [1]-[7]. In this respect, accurately calculating GIC is of great importance for assessing the effect of GMD on the power system.

In fact, the earth model, the geomagnetic field and the electric parameters of power system are the three primary factors during the GIC calculating procedure. In 2012, a benchmark test case was provided to facilitate the testing of GIC modeling procedures [8]. Following this benchmark, several researchers have devoted themselves to elaborating it in order to accord with practical situations [9]-[16]. For the earth model, a detailed 1-D layered earth model with flat layers of varying thicknesses and conductivity levels was firstly developed [17]; then a 3-D earth model is studied to quantify the impact of a geomagnetic storm [18]-[19]. But all the above studies have one thing in common: the earth model and the geomagnetic field are both regarded as uniform along the transmission line (TL).

However, for a high voltage power system with TLs over hundreds or even thousands of kilometers, the geological parameters and geomagnetic field will change significantly in most cases. So, it is essential to consider the variation of geological parameters and geomagnetic field along the TLs when calculating GIC. But limited earth survey sites and geomagnetic observatories have restricted this procedure.

To solve this problem, some literatures have made some efforts. [20] has used piecewise layered earth models to approximate the geological variations over the route of TL, which has a significant influence on the calculated GIC compared with using the laterally uniform earth model. [21] has calculated and compared the voltages across TLs using regional 1-D impedances and 64 empirical 3-D impedances obtained from a magnetotelluric survey. It also showed that the use of varying 3-D impedances along the TLs produces more spatial variance. In [22], the impact of various geoelectric field calculation methods on the GIC calculation is evaluated by comparison with the observations from a geomagnetic storm. The results showed that the spatially interpolated E-fields have produced closer agreement. Nevertheless, only the variation of the geological model is considered in these researches.

So, a more applicable GIC calculation method which considers the variation of both geological parameters and geomagnetic field should be proposed. As the earth survey sites and geomagnetic observatories are normally not located in the same position, it is necessary to interpolate them along the TL respectively. Considering the Tobler's first law of geography, both the magnetic field and ground model are believed to have spatial correlation in our problem [23]. In fact, results from [24] also showed the general falloff of correlative fidelity in the neutral currents as a function of distance from magnetometer to neutral current measurement location. So, a geostatistical interpolation method with the characteristic of spatial

This work is supported by National Key R&D Program of China under Grant 2016YFC0800100.

Yu-hao Chen, Yan-zhao Xie (corresponding author), Min-zhou Liu, Zong-yang Wang and Ai-ci Qiu are with the State Key Laboratory of Electrical Insulation and Power Equipment, School of Electrical Engineering, Xi'an Jiaotong Univeristy, Xi'an, Shaanxi Province, China (e-mail: chenyuhao@stu.xjtu.edu.cn, yzxie@xjtu.edu.cn).

Qing Liu is with the College of Electrical and Control Engineering, Xi'an University of Science and Technology, Xi'an 710054, China (e-mail: liuqing623nn@163.com).

autocorrelation should be adopted to deal with our problem. In fact, Kriging is a representative of the geostatistical interpolation methods [25]-[26]. Compared with other geostatistical interpolation methods, such as Thiessen polygons and inverse distance weight, it has the higher approximation degree, higher calculation ability and wider range of application [27]. After much improvement by many researchers, it has been widely applied in the fields of engineering science and natural science [28]-[30]. It not only provides the mean function to approximate the objective function but also the Kriging variance to represent the uncertainty of the model. So, the Kriging method is applied in this paper.

This paper is organized as follows. Section II firstly reviews the universal GIC calculation procedure. Then the application of Kriging interpolation in GIC calculation is introduced in section III, where the whole proposed calculation flow is summarized. To verify the feasibility of the proposed method, the GICs in Central China 1000 kV UHV grid is studied in section IV. Finally, section V concludes this paper with final remarks.

## II. Calculation Procedure of GIC

In theory, there are mainly three steps to calculate the GIC along the TL. The first step is to calculate the geoelectric field near the surface of the earth based on the measured geomagnetic field. Two methods are mostly adopted to describe their relationship: the surface impedance of the earth and the finite element model [31]. For the surface impedance tensor, the 1-D tensor derived from the multi-layer earth conductivity model has two opposite components while the 3-D tensor has four different components.

$$\boldsymbol{Z}_{1\mathrm{D}}=\begin{bmatrix}0 & Z\\ -Z & 0\end{bmatrix}\quad \boldsymbol{Z}_{3\mathrm{D}}=\begin{bmatrix}Z_{nn} & Z_{ne}\\ Z_{en} & Z_{ee}\end{bmatrix} \tag{1}$$

where $n$ indicates north and $e$ indicates east.

With the surface impedance tensor, the geoelectric field can be calculated based on (2) in the frequency domain.

$$\boldsymbol{E}(\omega)=\boldsymbol{Z}(\omega)\boldsymbol{B}(\omega)/\mu \tag{2}$$

where $\boldsymbol{E}(\omega)=[E_n(\omega),\ E_e(\omega)]^T$, $\boldsymbol{B}(\omega)=[B_n(\omega),\ B_e(\omega)]^T$; $\mu$ is the local magnetic permeability which is commonly regarded as free space value $\mu_0=4\pi\times10^{-7}$ H/m.

On the other hand, a 3-D earth conductivity finite element model can be normally built in a finite element software, such as ANSYS and COMSOL [32]. By applying geomagnetic field, the induced geoelectric field can be calculated with Maxwell's equation by a numerical analysis of the finite element.

The second step is to obtain the voltage between two substations by integrating the geoelectric field along the TL, which is described as (3).

$$U(\omega)=\int_L \boldsymbol{E}(\omega)\cdot d\boldsymbol{l} \tag{3}$$

where $L$ is the path of TL, $d\boldsymbol{l}$ is the path segment of TL.

Whether the surface impedance of the earth or the finite element model is used, the geoelectric field can always be decomposed into $E_n(\omega)$ and $E_e(\omega)$ components. So (3) can be transformed into:

$$U(\omega)=\int_L E_n(\omega)\cdot dl_n+\int_L E_e(\omega)\cdot dl_e \tag{4}$$

where $l_n$ is the northward distance of TL and $l_e$ is the eastward distance of TL.

In some cases, both $E_n(\omega)$ and $E_e(\omega)$ can be further decomposed with real parts and imaginary parts:

$$\begin{aligned}\mathrm{Re}\left[U(\omega)\right]&=\int_L \mathrm{Re}\left[E_n(\omega)\right]\cdot dl_n+\int_L \mathrm{Re}\left[E_e(\omega)\right]\cdot dl_e\\ \mathrm{Im}\left[U(\omega)\right]&=\int_L \mathrm{Im}\left[E_n(\omega)\right]\cdot dl_n+\int_L \mathrm{Im}\left[E_e(\omega)\right]\cdot dl_e\end{aligned} \tag{5}$$

By carrying out the inverse Fourier transform, the induced voltage can be obtained in the time domain. Finally, by regarding the impact of the magnetic field variation as dc voltage sources in series with each of the transmission lines, the GICs from substations to ground can be obtained [33]. In this paper, the LP method presented by Lehtinen and Pirjola is applied [34].

$$\boldsymbol{I}=\left(\boldsymbol{E}+\boldsymbol{YZ}\right)^{-1}\boldsymbol{J} \tag{6}$$

where $\boldsymbol{I}$ is the vector of GICs from substations to ground; $\boldsymbol{E}$ is the unit matrix; $\boldsymbol{Y}$ is the network admittance matrix; $\boldsymbol{Z}$ is the earthing impedance matrix; $\boldsymbol{J}$ depends on the induced voltages along the transmission line and the line resistance.

## III. GIC Calculation using Kriging Interpolation

Based on the introduced calculation procedure of GIC, we can find that the earth geology model, the geomagnetic fields and the electric parameters of the power system are the three primary factors. However, as high-voltage TLs usually run hundreds or even thousands of kilometers, a lack of earth model data or the limited local geomagnetic stations may restrict the assessment of GIC. To solve this problem, a well-performed interpolation method of Kriging is introduced to support a continuous earth geology model or the geomagnetic fields along the TLs.

### A. Objective Function

For the earth geology model, the variant components along the TL could be interpolated in the frequency domain. And these interpolated components include a real part and an imaginary part of 1-D or 3-D surface impedance tensor. It should be noted that if the 1-D surface impedance tensor is applied, the boundary effect between different earth structures will be ignored with some errors. In this respect, the objective function for earth geology interpolation could be supposed as:

$$y_e=f(\boldsymbol{x},\omega) \tag{7}$$

where $\boldsymbol{x}=[x_n,\ x_e]\in\mathbb{R}^2$ is the Euclidean position of the map; $\omega$ is the frequency variable; $y_e\in\mathbb{R}$ is the output variable of the interpolated earth geology component.

For the geomagnetic field, as there are four frequency components in our problem, that is, $\mathrm{Re}[E_n(\omega)]$, $\mathrm{Im}[E_n(\omega)]$, $\mathrm{Re}[E_e(\omega)]$ and $\mathrm{Im}[E_e(\omega)]$, four Kriging interpolation models need to be built in the frequency domain. So, it will be more complex and may bring bigger errors accordingly. In this way, to simplify the modeling process and avoid excessive errors, the magnetic fields are interpolated in the time domain for the north component and the east component respectively in our study. So, its objective function could be supposed as:

$$y_m = f(\boldsymbol{x}, t) \tag{8}$$

where $t$ is the time variable; $y_m \in \mathbb{R}$ is the output variable of interpolated geomagnetic component.

As the earth could be regarded as an ellipsoid with a smaller radius at the pole than at the equator, it is essential to transfer the coordinate of latitude and longitude into Euclidean coordinate firstly. By specifying appropriate point of longitude $\alpha_0$ and latitude $\delta_0$ as the origin, other positions ($\alpha$, $\delta$) could be transferred based on (9). In this calculation procedure, the WGS84 earth model is used, where the equatorial radius is 6378.137 km, the polar radius is 6356.752 km and the eccentricity square is 0.00669437999014 [35].

$$\begin{aligned} x_n &= \left(111.133 - 0.56\cos(2\phi)\right)\cdot(\delta - \delta_0) \\ x_e &= \left(111.5065 - 0.1872\cos(2\phi)\right)\cdot\cos\phi\cdot(\alpha - \alpha_0) \end{aligned} \tag{9}$$

where $\phi=(\delta+\delta_0)/2$.

### B. Kriging Interpolation

In fact, the Kriging interpolation method is to build a surrogate model for the objective functions of (7) and (8). From the perspective of Kriging, $f(\boldsymbol{x})$ is supposed to be a Gaussian process and $f(\boldsymbol{X}_t)$ obeys a joint Gaussian distribution where $\boldsymbol{X}_t$ is the input of training sets with $n$ dimensions. In fact, a Gaussian process is completely specified by its mean function $m(\boldsymbol{x})$ and covariance function $k(\boldsymbol{x}, \boldsymbol{x}')$ [36]-[37]. It can be expressed as:

$$f(\boldsymbol{x}) \sim GP\left(m(\boldsymbol{x}), k(\boldsymbol{x}, \boldsymbol{x}')\right) \tag{10}$$

The mean function $m(\boldsymbol{x})$ represents the trend of Kriging which is usually defined as:

$$m(\boldsymbol{x}) = \boldsymbol{g}^{\mathrm{T}}(\boldsymbol{x})\boldsymbol{\beta} \tag{11}$$

where $\boldsymbol{g}^T(\boldsymbol{x})=[g_1(\boldsymbol{x}), \ldots, g_p(\boldsymbol{x})]$ is a repressor vector and $\boldsymbol{\beta}$ is a $p$ dimensions vector of regression parameters.

The covariance function $k(\boldsymbol{x}, \boldsymbol{x}')$ models the dependence between different values of Gaussian process $Z(\boldsymbol{x})$. It can be expressed as:

$$k(\boldsymbol{x}, \boldsymbol{x}') = \sigma^2 r(\boldsymbol{x}, \boldsymbol{x}'; \boldsymbol{\theta}) \tag{12}$$

where $\sigma^2$ and $\boldsymbol{\theta}$ are hyper-parameters of covariance function; $r(\boldsymbol{x}, \boldsymbol{x}'; \boldsymbol{\theta})$ is the correlation function which only depends on the distance between the input samples, that is, when the distance is 0, the correlation function equals 1 and when the distance approaches infinite, the correlation function equals 0.

Indeed, the covariance function is the most important part of a Gaussian process and there is a tight relation between the regularity of the considered Gaussian process and the regularity of the covariance function. Squared exponential covariance function, ν-Matern covariance function and γ-exponential covariance function are three widely used covariance functions and are listed below respectively.

*1) Squared exponential covariance function:*

$$k(\boldsymbol{x}, \boldsymbol{x}') = \sigma^2 \exp\left(-\frac{\|\boldsymbol{x} - \boldsymbol{x}'\|^2}{2\theta^2}\right) \tag{13}$$

where $\theta$ is the correlation length.

*2) ν-Matern covariance function:*

$$k(\boldsymbol{x}, \boldsymbol{x}') = \frac{2^{1-\nu}}{\Gamma(\nu)}\left(\frac{\sqrt{2\nu}\|\boldsymbol{x} - \boldsymbol{x}'\|}{\theta}\right)^{\nu} K_{\nu}\left(\frac{\sqrt{2\nu}\|\boldsymbol{x} - \boldsymbol{x}'\|}{\theta}\right) \tag{14}$$

where $\theta$ is the correlation length; ν is the regularity parameter; $K_\nu$ is the modified Bessel function; Γ is the Euler-Gamma function.

*3) γ-exponential covariance function:*

$$k(\boldsymbol{x}, \boldsymbol{x}') = \exp\left(-\left(\frac{\|\boldsymbol{x} - \boldsymbol{x}'\|}{\theta}\right)^{\gamma}\right) \quad 0 < \gamma \le 2 \tag{15}$$

where $\theta$ is the correlation length and $\gamma$ is the power exponent.

Based on the principle of Gaussian process, the predicted sets $\boldsymbol{x}_p$ and training sets $\boldsymbol{X}_t$ obey the joint Gaussian distribution. That is:

$$\begin{pmatrix} f(\boldsymbol{x}_p) \\ f(\boldsymbol{X}_t) \end{pmatrix} \sim \boldsymbol{N}\left(\begin{pmatrix} \boldsymbol{g}^{\mathrm{T}}(\boldsymbol{x}_p)\boldsymbol{\beta} \\ \boldsymbol{G}\boldsymbol{\beta} \end{pmatrix}, \sigma^2 \begin{pmatrix} 1 & r^{\mathrm{T}}(\boldsymbol{x}_p) \\ r(\boldsymbol{x}_p) & \boldsymbol{R} \end{pmatrix}\right) \tag{16}$$

where $\boldsymbol{G}=g^{\mathrm{T}}(\boldsymbol{X}_t)$ is the derived repressor vector of training sets; $\boldsymbol{r}(\boldsymbol{x}_p)=r(\boldsymbol{x}_p, \boldsymbol{X}_t; \boldsymbol{\theta})$ is the correlation vector between $\boldsymbol{x}_p$ and $\boldsymbol{X}_t$; $\mathbf{R}=r(\boldsymbol{X}_t, \boldsymbol{X}_t; \boldsymbol{\theta})$ is the correlation matrix between the training points.

In this respect, the conditional distribution $[f(\boldsymbol{x}_p) \mid \boldsymbol{X}_t, \boldsymbol{\beta}, \sigma^2, \boldsymbol{\theta}]$ also obeys the Gaussian distribution, whose mean and variance are derived as:

$$\hat{m}(\boldsymbol{x}_p) = \boldsymbol{g}(\boldsymbol{x}_p)\boldsymbol{\beta} + r^T(\boldsymbol{x}_p)\boldsymbol{R}^{-1}(\boldsymbol{Y}_t - \boldsymbol{G}\boldsymbol{\beta}) \tag{17}$$

$$\hat{s}^2(\boldsymbol{x}_p) = \sigma^2\left(1 - r^T(\boldsymbol{x}_p)\boldsymbol{R}^{-1}r(\boldsymbol{x}_p)\right) \tag{18}$$

The Kriging mean $\hat{m}(\boldsymbol{x}_p)$ is the surrogate model used to approximate the objective function $f(\boldsymbol{x}_p)$ and the Kriging variance $\hat{s}^2(\boldsymbol{x}_p)$ represents the model mean squared error. From (17) and (18), we can see that the mean function and the variance function not only depend on the distance between the predicted point and the training points but also the distance between the training points themselves.

To estimate the parameters ($\boldsymbol{\beta}$, $\sigma^2$, $\boldsymbol{\theta}$) in (17) and (18), the maximum likelihood estimation is generally applied. This means:

$$\hat{\boldsymbol{\beta}}, \hat{\sigma}^2, \hat{\boldsymbol{\theta}} = \arg\max \log P\left(\boldsymbol{Y}_t \mid \boldsymbol{X}_t, \boldsymbol{\beta}, \sigma^2, \boldsymbol{\theta}\right) \tag{19}$$

where

$$P\left(\boldsymbol{Y}_t \mid \boldsymbol{X}_t, \boldsymbol{\beta}, \sigma^2, \boldsymbol{\theta}\right) = N\left(\boldsymbol{Y}_t \mid \boldsymbol{g}\boldsymbol{\beta}, R\left(\boldsymbol{X}_t, \boldsymbol{X}_t \mid \boldsymbol{\theta}\right) + \sigma^2 \boldsymbol{I}_n\right) \tag{20}$$

The detailed estimation procedure could be referred to in [36]-[37].

Furthermore, to improve the accuracy and robustness of the Kriging model, the training samples should be normalized and transferred into the range of [0, 1] before estimating the hyper-parameters [38]. The normalization formula is:

$$x^k_{normalized} = \frac{x^k - \min\left(\boldsymbol{x}^k\right)}{\max\left(\boldsymbol{x}^k\right) - \min\left(\boldsymbol{x}^k\right)} \tag{21}$$

where $x^k_{normalized}$ is the normalized result of the $k^{th}$ dimension input sample $x^k$ ($k$=1, 2, … , $n$); $\boldsymbol{x}^k$ is the the sample vector of the $k^{th}$ dimension input.

On the other hand, when we predict the features along lines using the built Kriging models, short lines generally result in

uniform distribution and cause some errors. In this respect, to avoid excessive error, the minimum length of lines should be no less than 1/20 of the minimum spatial distances between geomagnetic observatories and geological prospecting points.

### C. Summary of Proposed Algorithm

Based on the above introduced techniques, the flow of GIC calculation using the Kriging interpolation could be summarized in Fig. 1. Depending on whether the geomagnetic field data or the earth conductivities are limited, the Kriging interpolation is employed correspondingly.

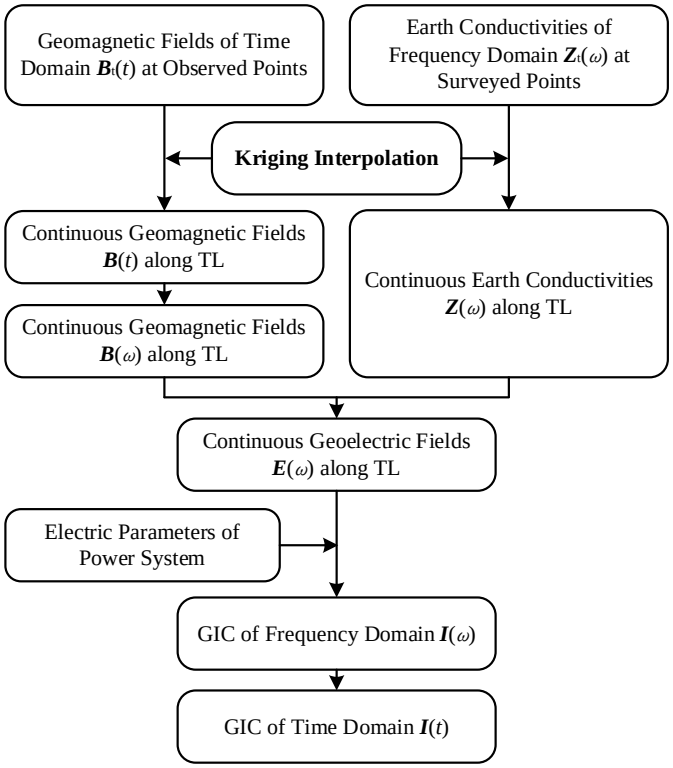


Fig. 1. Flow diagram of GIC calculation using Kriging interpolation.

## IV. Case Study

In this section, the Central China 1000 kV UHV grid is studied by interpolating both the geological model and the geomagnetic field based on the Kriging method. The map of the studied power system is shown in Fig. 2 and it mainly includes eight TLs and nine substations. Based on (9), its corresponding Euclidean coordinate is obtained in Fig. 3, where the point (110 °E, 25 °N) is set as the origin of coordinate.

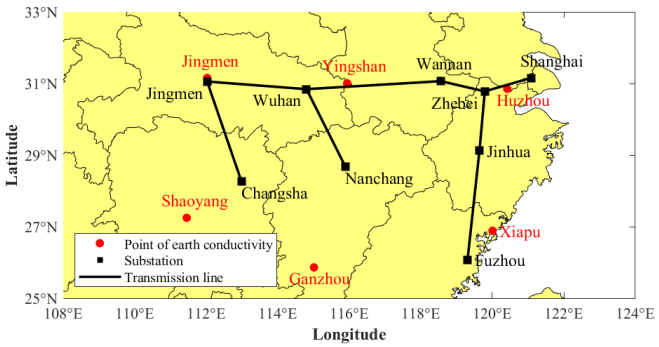


Fig. 2. The map of 1000 kV UHV transmission lines in Central China grid.

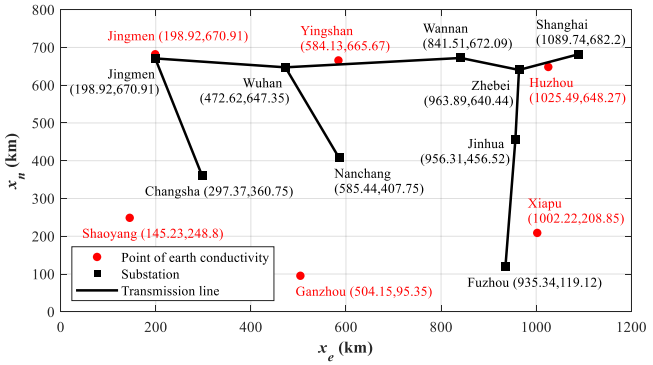


Fig. 3. The Euclidean coordinate of 1000 kV UHV transmission line in Central China grid.

Six 1-D earth models of Jingmen (JM), Yingshan (YS), Huzhou (HZ), Shaoyang (SY), Ganzhou (GZ) and Xiapu (XP) labeled in Fig. 2 are used to interpolate the surface impedance tensors along TLs using the Kriging method. And their detailed parameters are shown in TABLE I [39].

TABLE I
1-D Earth Models of Jingmen, Yingshan, Huzhou, Shaoyang, Ganzhou and Xiapu

| Depth (km) | JM (Ωm) | YS (Ωm) | HZ (Ωm) | SY (Ωm) | GZ (Ωm) | XP (Ωm) |
|---|---|---|---|---|---|---|
| 0~2 | 78 | 11524 | 216 | 24222 | 9123 | 6366 |
| 2~5 | 21 | 63783 | 4780 | 7133 | 6351 | 5557 |
| 5~10 | 22 | 132480 | 13289 | 2958 | 3130 | 6076 |
| 10~20 | 14 | 142670 | 13822 | 717 | 892 | 658 |
| 20~30 | 61 | 46921 | 4214 | 4574 | 417 | 1045 |
| 30~50 | 49 | 2744 | 361 | 4529 | 271 | 1138 |
| 50~70 | 2.4 | 1481 | 435 | 806 | 320 | 1579 |
| 70~100 | 0.15 | 269 | 506 | 15706 | 712 | 6452 |
| 100~150 | 0.11 | 231 | 69 | 41883 | 383 | 3734 |
| 150~200 | 0.08 | 692 | 17 | 28982 | 119 | 181 |
| 200~250 | 0.08 | 1387 | 135 | 8074 | 130 | 1016 |
| 250~300 | 0.08 | 1123 | 155 | 797 | 45 | 2588 |
| 300~∞ | 0.08 | 40 | 155 | 797 | 5000 | 900 |

For 1-D earth model with $m$+1 layers, the surface impedance tensor in (1) could be obtained by iteration layer by layer. And the relationship between surface impedances of adjacent layers is [40]:

$$Z_i(\omega)=\eta_i\frac{1+\dfrac{Z_{i+1}(\omega)-\eta_i}{Z_{i+1}(\omega)+\eta_i}e^{-2\gamma_i h_i}}{1-\dfrac{Z_{i+1}(\omega)-\eta_i}{Z_{i+1}(\omega)+\eta_i}e^{-2\gamma_i h_i}} \tag{22}$$

where $i$ is the label of layers and $i$=$m$, $m$-1, …,1; $h_i$ is the thickness of layer $i$; $\gamma_i$ and $\eta_i$ are the propagation constant and the intrinsic impedance of layer $i$, which are obtained by:

$$\gamma_i=\sqrt{j\omega\mu\sigma_i},\quad \eta_i=\sqrt{\frac{j\omega\mu}{\sigma_i}} \tag{23}$$

where $\mu$ is the permeability of free space; $\sigma_i$ is the conductivity of layer $i$.

By applying (22), the real and imaginary parts of surface impedances in Jingmen, Yingshan, Huzhou, Shaoyang, Ganzhou and Xiapu are shown in Fig. 4.

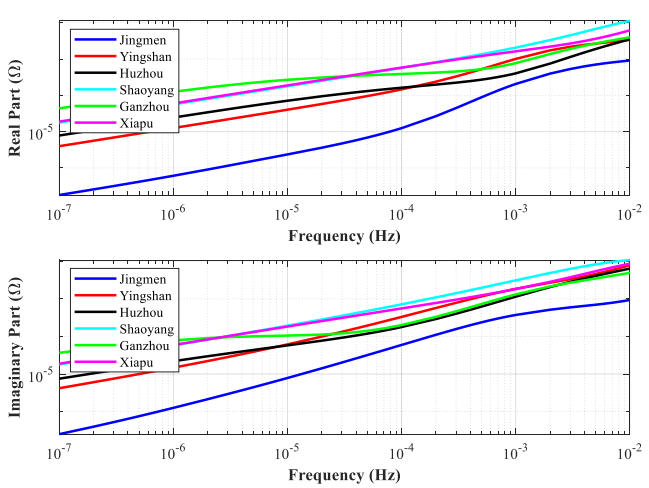


Fig. 4. The surface impedances of Jingmen, Yingshan, Huzhou, Shaoyang, Ganzhou and Xiapu.

Using Kriging interpolation with squared exponential covariance function, the surface impedance along the eight TLs in the frequency domain can be obtained based on these six known surface impedances. The interpolated real parts and imaginary parts of four typical TLs are shown in Fig. 5, respectively, where the abscissa is the position of TL and the ordinate is the spectrum distribution.

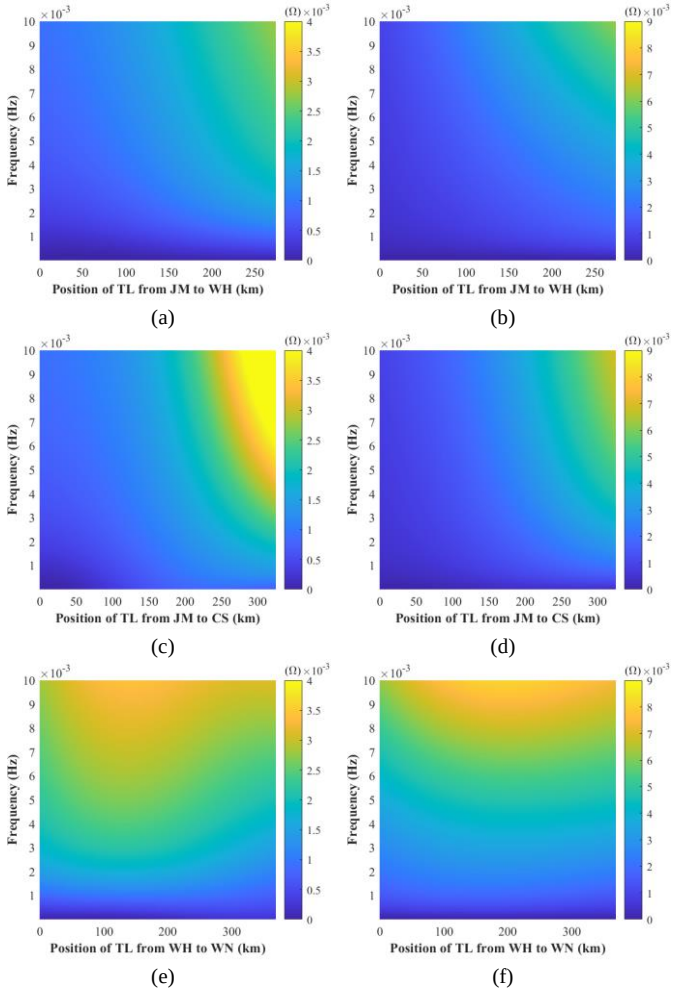


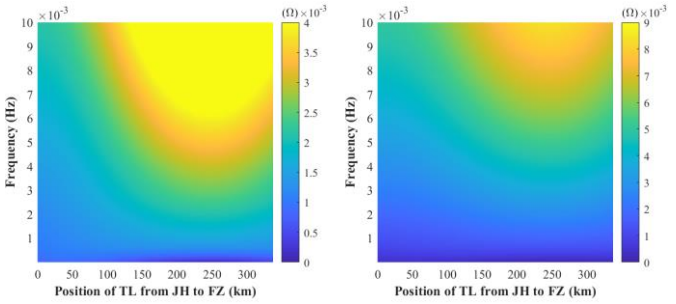


Fig. 5. The interpolated surface impedances along four typical TLs. (a) Real part of surface impedances from JM to WH, (b) Imaginary part of surface impedances from JM to WH, (c) Real part of surface impedances from JM to CS, (d) Imaginary part of surface impedances from JM to CS, (e) Real part of surface impedances from WH to WN, (f) Imaginary part of surface impedances from WH to WN, (g) Real part of surface impedances from JH to FZ, (h) Imaginary part of surface impedances from JH to FZ.

As for the geomagnetic field, a typical GMD event on November 6-19, 2004 is applied for final GIC calculation. Three different geomagnetic observatories are referred, namely, the observatory of Beijing Ming Tombs (BMT), the observatory of Lanzhou (LZH) and the observatory of Zhaoqing (GZH). Their positions are marked in Fig. 6 and the corresponding measured geomagnetic fields are shown in Fig. 7.

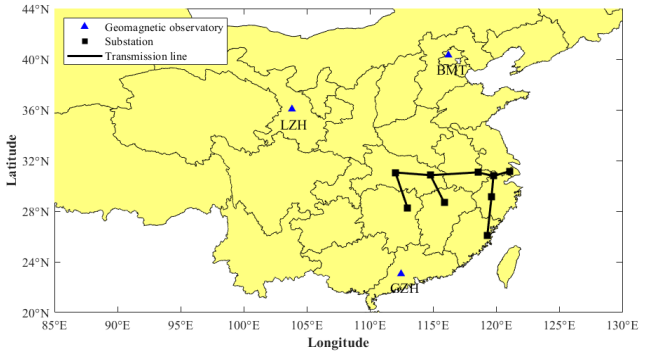


Fig. 6. The map of three different geomagnetic observatories.

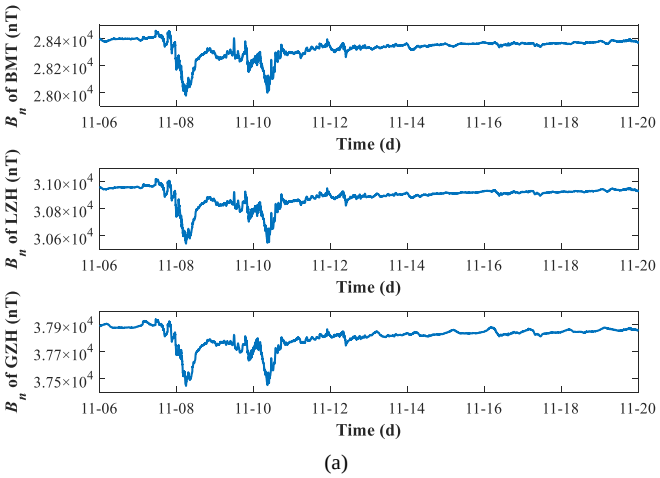

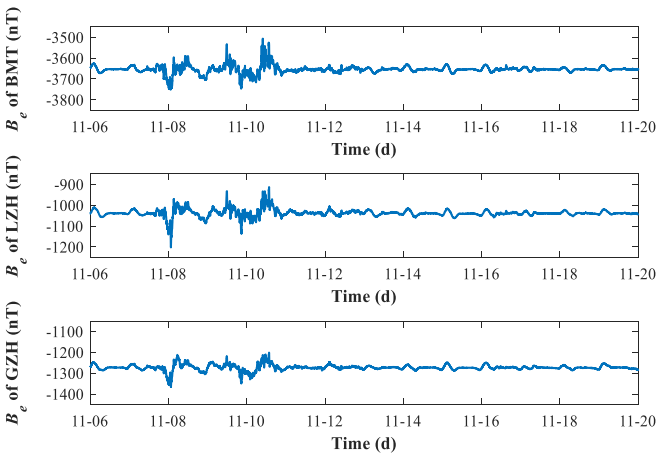


(b)

Fig. 7. The measured geomagnetic field of BMT, LZH and GZH observatories on November 6-19, 2004. (a) North component and (b) East component.

The interpolated geomagnetic fields of both north component and east component along the TLs are obtained by modelling the Kriging models of these measured results. During this process, the 5/2 Matern covariance function is adopted.

Finally, the GICs from each substation to ground could be calculated based on (2)~(6). During this procedure, the dc resistance of each TL phase is set as 0.0095 Ω/km; the dc resistance per phase of transformer consists of the series winding of 182.7 mΩ and the common winding of 141.5 mΩ; the typical grounding resistance of each substation is 0.1 Ω. The maximum GICs of each substation using interpolated geomagnetic model and different geomagnetic fields are shown in Fig. 8.

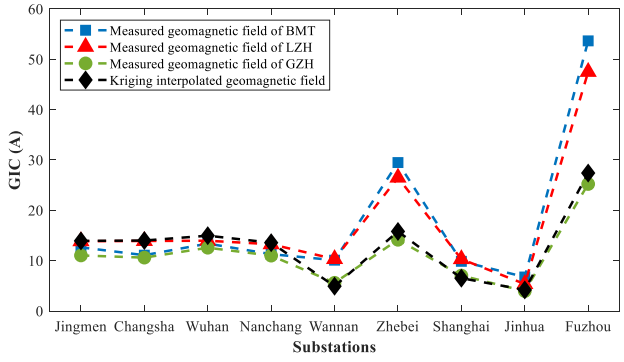


Fig. 8. The calculated maximum GIC from each substation to ground in 1000 kV UHV Central China grid using different geomagnetic fields.

From Fig. 8, we can observe that the GICs of Fuzhou and Zhebei substations are relatively higher than other substations and more sensitive to the geomagnetic field, which is a result of the power grid structure. On the other hand, the geomagnetic fields of BMT and LZH cause higher GICs than the fields of GZH. This could be explained by the fact that BMT and LZH are both located in the high-latitude region which has relatively more intense storms while GZH is located in the low-latitude area with weaker storms. And the GICs from Kriging interpolation are close to the ones from using just GZH measurements in some eastern substations, like Wannan, Zhebei, Shanghai, Jinhua and Fuzhou substations. This is because the distances from GZH to these eastern TLs are shorter than the ones from BMT and LZH to these eastern TLs, especially the TLs from Zhebei to Fuzhou. So, the GIC results of these eastern substations from Kriging interpolation are more likely to be influenced by the measurements of GZH. In this respect, by using Kriging interpolated geomagnetic field, we can clearly see that the results have fused the information from different geomagnetic observatories and they are generally among the results using geomagnetic fields of single observatory. Based on this, more reasonable threat assessment of GMD on the Central China 1000 kV UHV grid could be made.

## V. Conclusion

During the GIC calculation process, the earth conductivity model and the geomagnetic field are two critical factors. For high-voltage TLs of long length, the variations of these two factors should be considered instead of just using a uniform model. However, lack of data for either of them will influence the final assessment results.

In this respect, this paper introduces the Kriging method to interpolate the limited earth conductivity points or geo-magnetic observatories. By considering the distance between the predicted points and the training points as well as the distance between the training points themselves, the values of unknown area are estimated. To illustrate the proposed method, a case study of Central China 1000 kV UHV grid has been studied under the threat of GMD event on November 6-19, 2004. Both the surface impedances and geomagnetic fields are interpolated and the calculated GICs are compared by using different geomagnetic fields.

For further study, the GIC predicted by the proposed method will be compared with the measured result from a real geomagnetic storm to validate the effectiveness of the method.

## References

[1] D. Boteler, R. Pirjola, and H. Nevanlinna, "The effects of geomagnetic disturbances on electrical systems at the Earth's surface," *Adv. Space Res*., vol. 22, pp. 17-27, 1998.

[2] R. Pirjola, "Geomagnetically Induced Currents During Magnetic Storms," *IEEE Trans. Plasma Sci*., vol. 28, no. 6, pp. 1867-1873, Dec. 2000.

[3] L. Bolduc, P. Langlois, D. Boteler, and R. Pirjola, "A study of geoelectromagnetic disturbances in Québec, 1. General Results," *IEEE Trans. Power Delivery*., vol.13, no. 4, pp.1251-1256, 1998.

[4] L. Bolduc, P. Langlois, D. Boteler, and R. Pirjola, "A study of geoelectromagnetic disturbances in Québec, 2. Detailed Analysis of a Large Event," *IEEE Trans. Power Delivery*., vol.15, no. 1, pp. 272-278, 2000.

[5] D. Boteler, R. Pirjola, Ari Viljanen, and Olaf Amm, "Prediction of Geomagnetically Induced Currents in Power Transmission System", *Adv. Space Res*. vol. 26, no. 1, pp. 5-14, 2000.

[6] V. V. Vakhnina, V. A. Shapovalov, V. N. Kuznetsov and D. A. Kretov, "The Influence of Geomagnetic Storms on Thermal Processes in the Tank of a Power Transformer," *IEEE Trans. Power Delivery*., vol. 30, no. 4, pp. 1702-1707, 2015.

[7] W. A. Radasky, "Impacts of variations of geomagnetic storm disturbances on high voltage power systems," *IEEJ Trans. Power & Energy*, vol. 133, no. 12, pp. 931-934, 2013.

[8] R. Horton, D. Boteler, T. J. Overbye, R. Pirjola and R. C. Dugan, “A test case for the calculation of geomagnetically induced currents,” *IEEE Trans. Power Del.*, vol. 27, no. 4, pp. 2368-2373, Oct. 2012.
[9] K. Zheng, L. Trichtchenko, R. Pirjola and L. Liu, "Effects of geophysical parameters on GIC illustrated by benchmark network modeling", *IEEE Trans. Power Del.*, vol. 28, no. 2, pp. 1183-1191, 2013.
[10] K. Zheng, D. Boteler, R. J. Pirjola, L. Liu, R. Becker, L. Marti, S. Boutilier and S. Guillon, "Effects of system characteristics on geomagnetically induced currents", *IEEE Trans. Power Del.*, vol. 29, no. 2, pp. 890-898, 2014.
[11] S. Guo, L. Liu, R. Pirjola, K. Wang and Bo Dong, "Impact of the EHV power system on geomagnetically induced currents in the UHV power system", *IEEE Trans. Power Del.*, vol. 30, no. 5, pp. 2163-2170, 2015.
[12] M. Kazerooni, H. Zhu and T. J. Overbye, "Improved modeling of geomagnetically induced currents utilizing derivation techniques for substation grounding resistance", *IEEE Trans. Power Del.*, vol. 32, no. 5, pp. 2320-2328, 2017.
[13] D. Boteler and R. Pirjola, “Modeling geomagnetically induced currents,” *Space Weather*, vol. 15, no. 1, pp. 258-276, Jan. 2017.
[14] R. S. Weigel, “A comparison of methods for estimating the geoelectric field,” *Space Weather*, vol. 15, no. 2, pp. 430-440, Feb. 2017.
[15] C. Liu, X. Wang, S. Zhang and C.Xie, "Effects of lateral conductivity variations on geomagnetically induced currents: H-polarization", *Access IEEE*, vol. 7, pp. 6310-6318, 2019.
[16] Q. Liu, Y. Xie, N. Dong, Y. Chen, M. Liu and Q. Li, "Uncertainty quantification of geo-magnetically induced currents in UHV power grid", *IEEE Trans. Electromagn. Compat.*, vol. 62, no. 1, pp. 258-265, 2020.
[17] D. Boteler, “The evolution of Québec earth models used to model geomagnetically induced currents,” *IEEE Trans. Power Del.*, vol. 30, no. 5, pp. 2171-2178, Oct. 2015.
[18] P. A. Bedrosian and J. J. Love, “Mapping geoelectric fields during magnetic storms: synthetic analysis of empirical United States impedances,” *Geophys. Res. Lett.*, vol. 42, no. 23, pp. 10160-10170, Dec. 2015.
[19] A. Kelbert, C. C. Balch, A. Pulkkinen, G. D. Egbert, J. J. Love, E. J. Rigler and I. Fujii, “Methodology for time-domain estimation of storm time geoelectric fields using the 3-D magnetotelluric response tensor,” *Space Weather*, vol. 15, no. 7, pp. 874-894, Jun. 2017.
[20] L. Marti, C. Yiu, A. Rezaei-Zare and D. Boteler, “Simulation of geomagnetically induced currents with piecewise layered-earth models,” *IEEE Trans. Power Del.*, vol. 29, no. 4, pp. 1886-1893, Aug. 2014.
[21] G. M. Lucas, J. J. Love and A. Kelbert, “Calculation of voltages in electric power transmission lines during historic geomagnetic storms: an investigation using realistic earth impedances,” *Space Weather*, vol. 16, no. 2, pp. 185-195, Feb. 2018.
[22] R. Sun and C. Balch, “Comparison between 1-D and 3-D geoelectric field methods to calculate geomagnetically induced currents: a case study,” *IEEE Trans. Power Del.*, vol. 34, no. 6, pp. 2163-2172, Dec. 2019.
[23] W. R. Tobler, “A computer movie simulating urban growth in the Detroit region,” *Economic Geography*, vol. 46, no. 2, pp. 234-240, Jun. 2019.
[24] M. D. Butala, M. Kazerooni, J. J. Makela, F. Kamalabadi, J. L. Gannon, H. Zhu, T. J. Overbye, “Modeling geomagnetically induced currents from magnetometer measurements: spatial scale assessed with reference measurements,” *Space Weather*, vol. 15, no. 10, pp. 1357-1372, Oct. 2017.
[25] D. G. Krige, “A statistical approach to some mine valuation and allied problems on the Witwatersrand,” M.S. thesis, Faculty of Eng., University of the Witwatersrand, Witwatersrand, South Africa, 1951.
[26] G. Matheron, “Principles of geostatistics,” *Economic Geology*, vol. 58, no. 8, pp. 1246-1266, Dec., 1963.
[27] H. Li and Z. Shao, “Review of spatial interpolation analysis algorithm,” *Comp. Sys. and Appl.*, vol. 28, no. 7, pp. 1-8, Jul., 2019.
[28] J. Sacks, W. J. Welch, T. J. Mitchell and H. P. Wynn, “Design and analysis of computer experiments,” *Statistical Science*, vol. 4, no. 4, pp. 409-423, Nov., 1989.
[29] N. Cressie, “Spatial prediction and ordinary kriging,” *Math. Geol.*, vol. 20, no. 4, pp. 405-421, May, 1988.
[30] N. Cressie, “The origins of kriging,” *Math. Geol.*, vol. 22, no. 3, pp. 239-252, Apr. 1990.
[31] B. Dong, Z. Wang, D. Boteler and R. Pirjola, “Review of earth conductivity structure modelling for calculating geo-electric fields,” *IEEE Power & Energy Society General Meeting 2013*, 21-25, Jul. 2013.
[32] B. Dong, D. W. Danskin, R. Pirjola, D. Boteler and Z. Wang, “Evaluating the applicability of the finite element method for modelling of geoelectric fields,” *Ann. Geophys.*, vol. 31, no. 10, pp. 1689-1698, Oct. 2013.
[33] T. Overbye, T. Hutchins, K. Shetye, J. Weber and S. Dahman, "Integration of geomagnetic disturbance modeling into the power flow: a methodology for large-scale system studies," in *Proc. 2012 North American Power Symposium*, Champaign, IL, USA, 2012.
[34] M. Lehtinen and R. Pirjola, “Currents produced in earthed conductor networks by geomagnetically induced electric fields,” Annales Geophysicae, vol. 3, no. 4, pp. 479-484, Jan. 1985.
[35] R. H. Rapp, Geometric Geodesy Part 1, Dept. Geodetic Sci. Surveying, Ohio State Univ., Columbus, course notes, 1994. [Online]. Available: http://hdl.handle.net/1811/24333.
[36] C. E. Rasmussen and C. K. I. Williams, *Gaussian Processes for Machine Learning*. MIT Press, Cambridge, Massachusetts, 2006.
[37] L. L. Gratiet, “Multi-fidelity Gaussian process regression for computer experiments,” Ph.D. dissertation, Autres [stat. ML]. Universite Paris-Diderot - Paris VII, Francais, <tel-00866770v1>, 2013.
[38] Z. Han, “Kriging surrogate model and its application to design optimization: A review of recent progress,” *Acta Aeronautica et Astronautica Sinica*, vol. 37, no. 11, pp. 3197-3225, Nov. 2000.
[39] K. Zheng, “Research on influence factors and modelling methods of geomagnetically induced currents in large power grid,” *Ph.D. dissertation*, North China Elect. Power Univ., Beijing, China, 2014.
[40] L. Marti, A. Rezaei-Zare and D. Boteler, “Calculation of induced electric field during a geomagnetic storm using recursive convolution,” *IEEE Trans. Power Del.*, vol. 29, no. 2, pp. 802-807, Apr. 2014.

**Yu-hao Chen** was born in Shaanxi, China, in 1993. He received the B.Sc. degree and Ph.D degree in electrical engineering from Xi’an Jiaotong University, Xi’an in 2015 and 2021 respectively. He is currently an assistant professor of school of electrical engineering, Xi’an Jiaotong University.

His research interests include effect evaluation of high-altitude electromagnetic pulse and geomagnetic storm.

**Yan-zhao Xie** (M’12-SM’19) was born in Henan, China in 1973. He received the Ph.D. degree in electrical engineering from Tsinghua University, Beijing, China, in December, 2005. He is currently a Professor of School of Electrical Engineering, Xi'an Jiaotong University, China.

His research interests include multi-conductor transmission lines analysis, electromagnetic time reversal technique, electromagnetic transients in power system and high-power electromagnetics, etc.

**Min-zhou Liu** was born in Hebei, China, in 1995. He received the B.Sc. degree in electrical engineering from Xi'an Jiaotong University in 2017, where he is currently working toward the M.S. degree. His research interests include effects evaluation of electromagnetic environments and reliability evaluation of power system.

**Zong-yang Wang** was born in Henan, China, in 1997. He received the B.Sc. degree in electrical engineering from North China Electric Power University, Beijing, China, in 2019. He is currently pursing the Ph.D. degree in electrical engineering in Xi'an Jiaotong University.

His research interests include effect evaluation of high-altitude electromagnetic pulse and geomagnetic storm.

**Qing Liu** was born in in 1978. She received the B.Sc. degree in electrical engineering from Chongqing University in 2000 and received M.S. degree and Ph.D degree in electrical engineering from Xi'an Jiaotong University in 2005 and 2020 respectively. She is also an associate professor in Xi'an University of Science and Technology. Her research interest includes modeling and assessing geomagnetically induced currents in the power grid.

**Aici Qiu** was born in Zhejiang, China, in November 1941. She received the B.E. degree in electrical engineering from Xi'an Jiaotong University (XJTU), Xi'an, China, in 1964.

She is currently a Professor with XJTU. She was elected as a member of the Chinese Academy of Engineering in 1999. She has been working on pulse-power technology and intense current pulse particle beam accelerator for more than five decades.